On the stability of hollow nanoparticles and the simulation temperature ramp

Journal:	*Inorganic Chemistry Frontiers*
Manuscript ID	QI-RES-12-2017-000822.R1
Article Type:	Research Article
Date Submitted by the Author:	17-Feb-2018
Complete List of Authors:	Reyes, Paula; Facultad de Ciencias Universidad de Chile, Physics Valencia, Felipe; Faculatd de Ciencias, Universidad de Chile, Physics Vega, Hector; Facultad de Medicina, Universidad de Chile, Instituto de Ciencias Biomedicas Ruestes, Carlos; Universidad Nacional de Cuyo Rogan, Jose; Facultad de Ciencias, Universidad de Chile, Physics Valdivia, Juan; Facultad de Ciencias, Universidad de Chile, Physics Kiwi, Miguel; Facultad de Ciencias, Universidad de Chile, Physics

Journal Name

ARTICLE TYPE

Cite this: DOI: 10.1039/xxxxxxxxxx

On the stability of hollow nanoparticles and the simulation temperature ramp

Paula N. Reyes,[a,b] Felipe J. Valencia,[a,b,c] Hector Vega,[d] Carlos Ruestes,[e] Jośe Rogan,[a,b] J. A. Valdivia[a,b] and Miguel Kiwi[a,b]

Received Date
Accepted Date

DOI: 10.1039/xxxxxxxxxx

www.rsc.org/journalname

Hollow nanoparticles (hNPs) are of interest because their large cavities and small thickness give rise to a large surface to volume ratio. However, in general they are not in equilibrium and far from their global energy minimum, which often makes them unstable against perturbations. In fact, a temperature increase can induce a structural collapse into a nanoparticle, and consequently a loss of their unique properties. This problem has been studied by means of molecular dynamics (MD) simulations, but without emphasis on the speed of the temperature increase. Here we explore how the temperature variation, and the rate at which it is varied in MD simulations, determines the final conformation of the hNPs. In particular, we show how different temperature ramps determine the final shape of Pt hNPs that initially have an external radius between 0.7 and 24 nm, and between 0.19 and 2.4 nm internal radii. In addition, we also perform simulations of other similar metals like Ag and Au. Our results indicate that the temperature ramp strongly modifies the final hNP shape, even at ambient temperature. In fact, a rapid temperature increase leads to the formation of stacking faults and twin boundaries which are not generated by a slower temperature increase. Quantitative criteria are established and they indicate that the stacking fault energy is the dominant parameter.

1 Introduction

Hollow cavity nanoparticles (hNPs) have recently attracted significant interest. However, their stability,[1–3] thermal behavior,[4–7] and mechanical properties[8,9] has not been investigated in great detail. hNPs have been synthesized because of their high performance in catalysis processes,[3] gas storage capability, plasmonics, gas sensing,[10,11] and drug delivery,[12,13] among other important applications. Consequently, abundant experimental results are available for hNPs synthesized with various shapes and sizes.[14] Several shapes that have been studied such as cubes, octahedra, prisms, nanocages,[15–17] and nanoframes, among others.[18] Their sizes range from the nano- to the micro-scale. Since hNP are highly porous they are promising materials in many fields, and the proper modeling of these structures is a useful tool in the study of their response under different demands.[3,19]

The simulations of hNPs that have been reported start from a configuration that is obtained by cutting two concentric spheres, with given internal and external radii, in the bulk material. However in general this procedure yields structures that are far from equilibrium, since the surfaces that are created are arbitrary, and reflect the presence of stress remnants. Consequently, a better choice is to implement an energy minimization algorithm that effectively relaxes the system; however, if the energy barrier is small, this procedure does induce the hNP collapse. A different approach, and also the most usual one, is to raise the temperature following a slow temperature ramp to allow for atomic rearrangement.[2,4–7] Quite often the temperature ramp that is adopted raises the temperature linearly from 0 to 300 K in 0.2 ns. Unfortunately the choice of a particular temperature ramp leads to different results when starting from a far from equilibrium conformation.

The energy and stress dissipation speeds, as well as the surface reconstruction for hNPs, are not necessarily the same for a large or bulk system. In fact, they are key factors in defect generation by sliding planes, and the subsequent formation of stacking faults (SFs) and/or twins.[2] This topic is the main concern of this paper, and can be formulated as follows: how does the temperature ramp influence the results of the simulations? Our main objective is to provide a quantitative analysis in order to establish the largest temperature increase speed that provides reliable thermodynamic results.

The stability of hNPs was addressed by Jiang *et al.*,[2] who put forward three possible characterizations for an initial configuration: i) stable, if the initial configuration keeps its initial shape; ii) half-stable, if a partial collapse occurs, but the cavity is preserved; and, iii) unstable if the hNP collapses into a solid NP.

To display these characterizations they used a two dimensional phase diagram that will be explained below. Recently Jiang *et al.*[5] also investigated the role of temperature on the phase diagram. In both of these papers the final quasi-equilibrium state that is reached is attributed to the combination of the hNP wall thickness, the external radius and a thermal factor. However, several authors reported the thermal properties of these hNPs but did not emphasize, or completely ignored, the choice of the temperature ramp.[3,5,6]

Since Pt is one of the most important materials that is used both in catalytic processes and to store gases, particularly H, our focus of attentions to model the thermal stability of Pt hNPs by means MD simulations. To do so we construct three different stability diagrams for this system following the procedure of Jiang *et al.*[2]; each of these diagrams corresponds to a different temperature ramp, aiming to establish how they determine the final structures. We observe that the strain dissipation plays a key role in the defect formation of stacking faults (SFs), and in the collapse of the hNP into a solid Pt NP.

It is worth remarking that the subject of hNPs has very recently received much attention. In particular, Akbarzadeh *et al.*[20] studied AuAg hNPs by means of similar techniques to the ones we implement here, and they also reported results on the stability of Ni-Pd hNPs.[21] They modeled single size systems of different morphologies and concluded that they are unstable at room temperature, collapsing into NPs. Here we generalize to various different size systems, and subject to different temperature schedules; moreover, we also compare our results by simulations of other elements.

Laser ablation has been employed as a technique to produce hollow nanostructures[22–28]; this way the laser induces electronic excitations of the NP which couple to the lattice heating the system. A detailed discus ion of the relation between electronic excitations and thermal effects was given by Gonzalez et al.[29]. Usually the pulse width employed changes in different expertiments. For example, Kim et al.[27] employed 10 ps pulses in the synthesis of Pt hNP, while Sen et al.[25] used 10 ns laser pulses in the synthesis of WS_2 and MoS_2 hNPs. The temperature can be rapidly raised to close to the melting point, and later dissipated to the surrounding material, usually a fluid. In these, experiments only a fraction of the nanoparticles adopt hollow structures. Here, in spite of the fact that we are far away from the temperatures achieved in laser ablation experiments, we observed that hNPs are strongly affected by rapid temperature increases. These results can help to elucidate how thermal effects control the synthesis of hNPs production.

2 Method

The thermal stability of different Pt hNPs is determined by means of MD simulations using the LAMMPS code.[30] The interaction between Pt atoms is modeled by means of the Embedded Atom Method Potential[31], using the parametrization by Sheng,[32], which yields satisfactory results for the elastic constants, Pt diffusion coefficient, and SF energies. There are more complex interatomic potential available in the literature, such as the Tersoff[33], COMB[34], and ReaxFF, among others. They usually include bond order, and/or charge transference terms. These potentials can be used for example to simulate molecules, small metallic clusters and chemical processes, which in general are not suited for treatment by an EAM potential. However, the hNPs studied here posses a larger number of atoms and a well defined crystalline structure; therefore, an EAM type potential can reproduce the same structural properties with a lower computational cost as compared with a reactive interatomic potential, which allows to simulate the behavior of larger hNPs over longer periods of time, the main purpose of this contribution. Each hNP was created cutting out two different radii concentric spheres in the face-centered cubic (fcc) Pt bulk. All hNPs initially have an external radius of $a_0 \leq R_{ext} \leq 60a_0$, and a thickness between $0.5a_0 \leq w \leq 6a_0$ respectively, where $a_0 = 3.92$ Å is the Pt lattice parameter. This choice leads to hNPs ranging from a hundred to a million atoms. The temperature of every structure is raised from 0 to 300 K by means of a velocity rescaling algorithm, using three different temperature ramps: 0.3, 1.5 and 30 K/ps, which in simulation times correspond to 0.01, 0.2 and 1.0 ns, respectively. When the desired temperature is reached the velocity rescaling algorithm is disconnected, and the hNP evolution is followed in the NVE ensemble during 0.2 ns in order to check the stability of the final configuration in the absence of a thermostat.

The structure and its defects were analyzed using the common neighbor analysis (CNA) algorithm, as implemented in the OVITO software.[35,36] More complex defects, such as dislocations, were studied using the Dislocations Extraction algorithm[36] (DXA). Planar defects, which correspond to hcp regions inside the fcc Pt lattice, were classified using the crystal analysis tool (CAT) algorithm in order to differentiate between SFs and twin boundaries. The radial pressure profiles were obtained from the stress tensor by means of the relation

$$p_i^{\alpha\beta} = -\frac{1}{3}\mathrm{Tr}\left[\frac{m_i v_i^\alpha v_i^\beta + \sum_{i\neq j} F_{ij}^\alpha r_{ij}^\beta}{\Omega_i}\right], \qquad (1)$$

where the first term is the thermal contribution of the stress tensor; v_i^α is the α-component of the velocity of the i-th atom; Ω_i is the atomic volume; and F_{ij}^α and r_{ij}^α correspond to the force and distance between atoms i and j, respectively. Under this definition a positive pressure is tensile, and a negative one is compressive.

3 Results

The stability diagrams we obtained, following the scheme by Jiang *et al.*[2] are displayed in Fig. 1. They illustrate the dependence on the temperature increase rate (different temperature ramps) that are chosen to reach thermal equilibrium of the system. In all the three cases we studied it is noticed that if the thickness is larger than $2a_0$, all the 81 hNPs we simulated preserve their hollow configuration. The main difference is the ratio of stable structures relative to the half stable ones. In fact, for the 30 K/ps ramp this ratio is $\approx$ 21%, while for the slower 1.5 K/ps temperature increase the ratio increases to 37%. When the even slower ramp of 0.3 K/ps is applied the ratio further increases to 50%. In all the cases mentioned above the half-stable structures are mainly due to planar defects, especially SFs, and a smaller

fraction is due to twins (when the hNP thickness is smaller). The transition occurs during the first picoseconds of the simulation, and can be attributed to a sudden kinetic energy increase related to atomic reordering, triggered by the stress due to the presence of the cavity.

It is quite apparent that a strong correlation exists between the way the temperature is increased and the fraction of stable and half-stable hNPs; namely a slow temperature increase favors the formation of stable hNPs, while a fast increase leads to predominantly half-stable configurations. A rapid temperature increase adds kinetic energy to the system without allowing enough time to reach quasi-equilibrium. However, if the kinetic energy is pumped slowly into the hNP surface reconstruction has enough time to take place, allowing the cavity surface to contract without the formation of planar defects. Thus, the generation of SFs is avoided, restricting the collapse into a solid NP. All of this allows us to establish that a hNP thickness w larger than twice the lattice parameter ($w > 2a_0 \approx 8$nm) constitutes a minimal requirement for their successful synthesis.

Fig. 2 illustrates the temperature vs. time results of an NVE simulation for hNPs of $w/a_0 = 1.5$, for which the three types of possible configuration outcomes are obtained (stable, half-stable and unstable). For the ratio $A = R_{ext}/w = 2$ and 3 the hNPs reach equilibrium after just a few picoseconds, and approach a constant final temperature below 300 K. However, for $A = 4,\ 5,\ 6$ and 7 the hNPs collapse within less than 20 ps into an unstable structure, rather than the half-stable one that is reached when coupled to a thermostat. As a consequence of the collapse, the hNP temperature increases reaching values close to the melting point. This constitutes an indication that some half-stable hNPs are due exclusively to the intervention of the thermostat, but cannot be stabilized once the crystal plane slip sets in.

In Fig. 3 we display the pressure profiles as a function of radius for hNPs of fixed thickness $w = 1.5a_0$. The dashed gray lines denote the initial pressure profile and show that the original system is always stressed, which reaches peaks in the vicinity of the inner and outer surfaces. After a few picoseconds most of the initial tensile stress is dissipated by the compression of the inner and outer surfaces of the hNP. Once the inner cavity is compressed, the shell atoms are also compressed, and the surface tensile peaks decrease due to surface reconstruction. This effect has been observed in many metallic surfaces, including thin films.[37]

In the stable configurations compressed atoms are present in the center layers, compensating the tensile deformation of both surfaces. In the case of half-stable configurations the shell is not able to withstand the surfaces stress. As a result, the hollow nanoparticle shrink increasing the shell thickness, and reducing the cavity size to compensate surface stress. Moreover, as shown in Fig. 3, there is no important difference between inner and outer surface peaks, which implies that there is little difference between the crystal structure of the inner and outer surfaces. This is in good agreement with XRD diffraction patterns obtained for Pt hNPs, and for several other metallic hNPs,[3] where characteristic diffraction peaks are observed.

The shear stress on the hNPs is illustrated in Fig. 4. In addition to pressure profiles studied previously the shear stress evolution

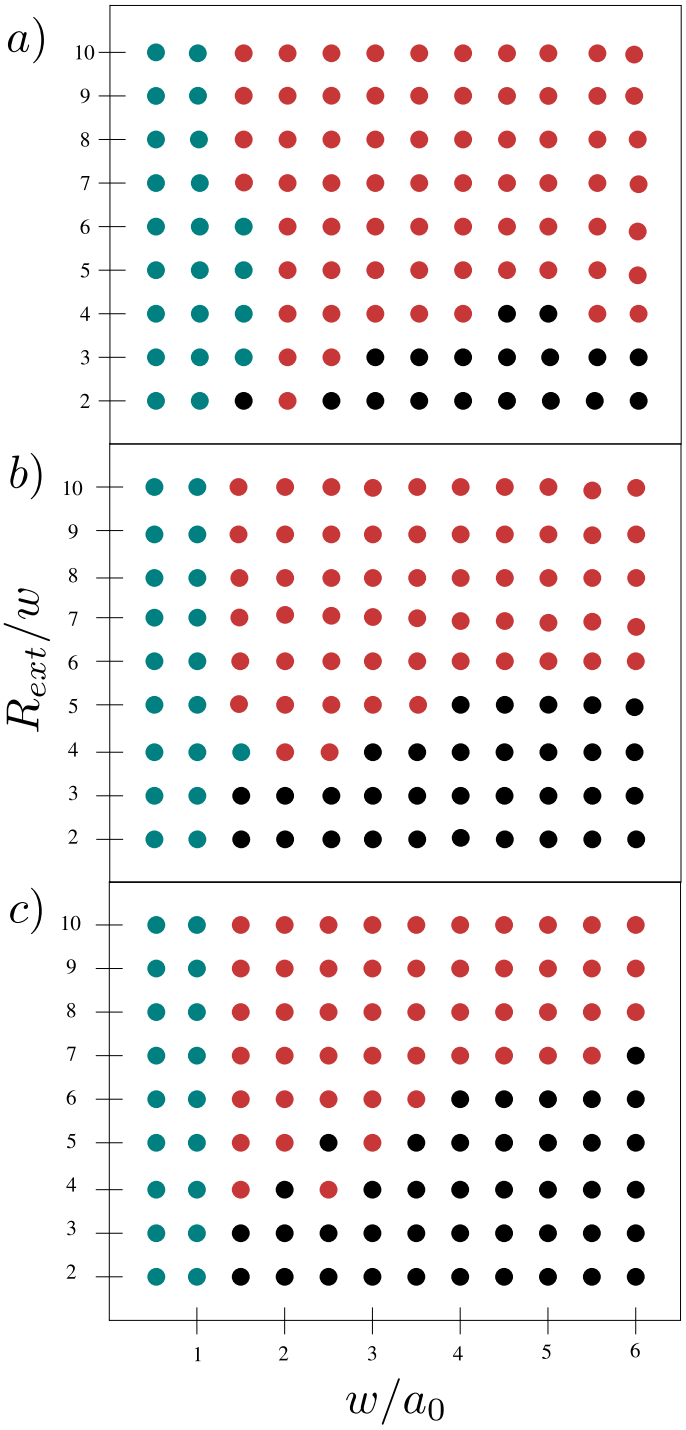

Fig. 1 Three different stability diagrams for temperature ramps of a) 30K/ps, b) 1.5K/ps and c) 0.3K/ps. Red, blue, and black circles correspond to half-stable, unstable and stable hNPs, respectively. w is the shell thickness, and R_{ext} is the external radius.

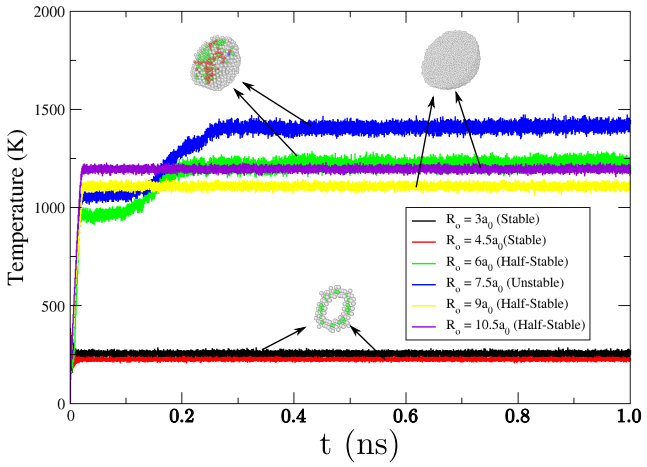

Fig. 2 Temperature as a function of time for hNPs with different aspects ratios. The thickness is set to $w/a_0 = 1.5$. The pictures illustrate a planar cut through the resulting structure, after a few picoseconds of simulation time. Red, green, and blue label hcp, fcc, and bcc crystalline structures, respectively, while the white atoms represent particles without a well defined crystal structure.

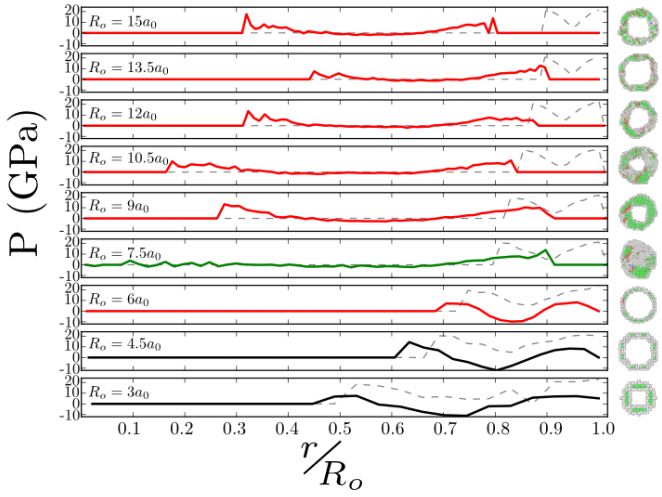

Fig. 3 Radial pressure profiles plots for a stable (black), half-stable (red) and unstable (green) hNP. The dashed gray lines correspond to the initial pressure profile and show that the original hNPs are always stressed, and this stress peaks in the vicinity of the inner and outer surfaces. Right panels show a CNA of the final configuration of every hNP; green and red atoms correspond to fcc and bcc, respectively.

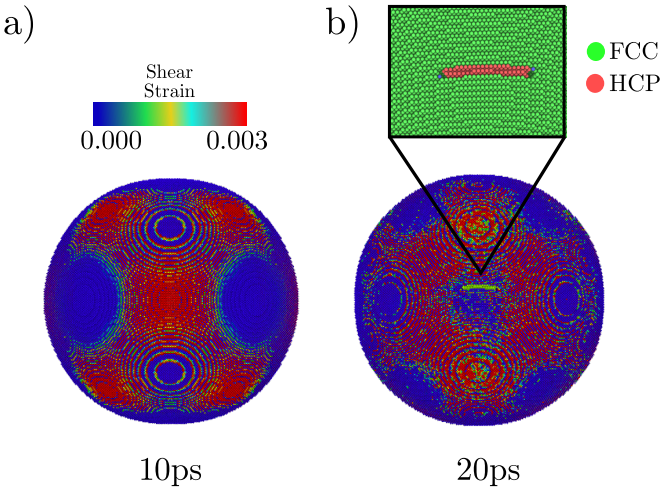

Fig. 4 Strain distribution on the outer hNP surface of a hNP of thickness $w = 5a_0$ and $R_{ext}/w = 7$. The temperature ramp is 0.3 K/ps. The color coding depicts the shear strain the Pt atoms suffer. Atoms in red are subject to large strain, while the blue ones are relaxed. After 20ps simulation time we show a CNA analysis of the dislocations; red and green atoms correspond to hcp and fcc, respectively.

provides information on the mechanisms on the involved in the hNP defect formation. In Fig. 4a there is a clear strain gradient on the hNP surface, with a shear stress acumulation along the [100] axis, and there is stress relaxed region on the {111} planes. After 10 ps the shear strain accumulation is distributed over the whole hNP resulting in the nucleation of a stacking fault on the [100] surface. This kind of failure is commonly observed in fcc NPs due the intersection of four {111} planes close to the [100] surface. The dislocation results in a SF delimited by the nucleation of two Shockley partial dislocations (inset in Fig. 4b), and the shear stress decreases in the region close to the SF. For longer simulation times the hNP keeps its shape, and no evidence for the formation of additional dislocations is observed.

A relevant issue is how general are the effects that we find changing the temperature ramp in the simulation of Pt hNPs. In fact, we expect them to apply to other elements as well, since they are important near the melting temperature. Therefore, we investigate the importance of the temperature ramp in the calculation of the SF energies of other metals, like Ag, Au, Pt_1 (this work) and Pt_2, where the latter two denote different Pt potentials[32,38] that were already used by other authors. In Fig. 5 we show the results of these simulations, which were carried out using temperature ramps of 0.3 K/ps and 1.5 K/ps, but with the same potentials used by the previous authors. It is noticed right away that three of the four cases mentioned above do depend on the speed of the temperature ramp. The Johnson *et al.*[39] and Foiles*et al.*[40] potentials yield an almost negligible SF energy per unit area γ_{SF}, which implies that small thermal fluctuations can stimulate a transition to half-stable hNPs by means of the nucleation of SFs. On the other hand, Pt_1 yields a γ_{SF} almost twice as large as the one obtained using[38] Pt_2, which implies that discrepancies in the stable/half-stable transition are to be expected.

Table 1 Stacking fault energies for Foiles *et al.*[40] (Au), Johnson *et al.*[39] (Au), Sheng *et al.*[32] (Pt_1) and Zhou *et al.*[38] (Pt_2) potentials.

	Ag		Au		Pt_1		Pt_2	
	Foiles	Exp.	Johnson	Exp.	Sheng	Exp.	Zhou	Exp.
γ_{SF} (mJ/m^2)	2	20	4	32	121	110	66	110

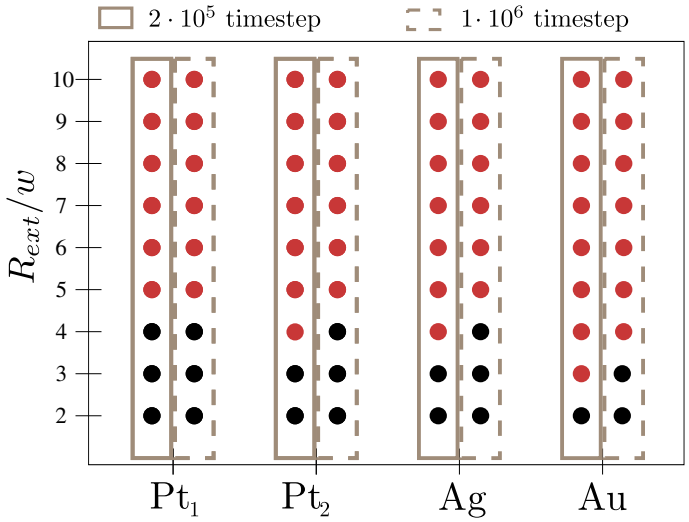

Fig. 5 Stability of hNPs of different metals, all of which have a width of $w = 3a_0$. Black and red represent stable and half-stable structures, respectively. The continuous and dashed regions correspond to a temperature ramp of $2{\cdot}10^5$ and $1{\cdot}10^6$ timesteps, respectively. Ag, Au, Pt_1 (this work) and Pt_2 label different potentials.

4 Summary and Conclusions

It is reasonable to think that molecular dynamics simulation of hollow nanoparticles could be highly dependent on the choice of the temperature ramp. Our data confirm this expectation, providing quantitative information and insight into the mechanisms by which the stability of the hNP final structure is achieved. It shows that slower temperature ramps generate less planar defects, in comparison with faster ramps which favor the formation of half-stable hNPs. The latter have a high population of SFs and twin boundaries. Even though stable hNPs are obtained using different temperature ramps, when the hNP thickness to radius ratio A (the aspect ratio) increases, the choice of the temperature ramp strongly influences the final hNP shape.

In the generated hole cavity positive pressure profiles are observed, due to the tensile strain induced in the shell, which is dissipated by the spherical compression and the surface rearrangement. In critical cases, when there is a rapid change in stress distribution, it is possible to observe the nucleation of Shockley partial dislocations during the first picoseconds of simulation. For large aspect ratios, they yield half-stable structures or the collapse into solid NPs. Experimental evidence of SFs and twin boundaries in half-stable hNPs have been previously reported; using TEM microscopy for many different metallic hNPs.[41,42] Their poly-crystalline nature was also observed, thus suggesting that half-stable hNPs are a more realistic model to understand experimental results.

While here we limited our attention to spherical geometry hNPs our conclusions apply as well to many highly porous structures,[43] such as hollow nanorods, hollow nanocubes,[44] hollow nanoprisms,[42] nanoframes,[45] nanofoams and others. When they are far from equilibrium the choice of how the temperature is rescaled is often critical, when attempting to properly model and simulate these nanostructures.

5 Acknowledgments

The authors thanks useful comments by Eduardo M. Bringa. This work was supported by the Fondo Nacional de Investigaciones Científicas y Tecnológicas (FONDECYT, Chile) under grant #1160639 (MK and JR), #1150718 (JAV) and Financiamiento Basal para Centros Científicos y Tecnológicos de Excelencia FB-0807 (FV, JR, JAV and MK). MK and FV were supported by AFOSR Grants FA9550-16-1-0122 and FA9550-16-1-0384. CJR thanks ANPCyT PICT-2015-0342. FV was supported by CONICYT Doctoral Fellowship grant #21140948. This research was partially carried out at the supercomputing infrastructure of the NLHPC (ECM-02).

References

1 S. S. Dalgic, *Acta Phys. Polonica A*, 2016, **129**, 531–534.
2 L. Jiang, X. Yin, J. Zhao, H. Liu, Y. Liu, F. Wang, J. Zhu, F. Boey and H. Zhang, *J. Phys. Chem. C*, 2009, **113**, 20193–20197.
3 A. Shan, Z. Chen, B. Li, C. Chen and R. Wang, *J. Mater. Chem. A*, 2015, **3**, 1031–1036.
4 F. J. Valencia, R. I. González, D. Tramontina, J. Rogan, J. A. Valdivia, M. Kiwi and E. M. Bringa, *J. Phys. Chem. C*, 2016, **120**, 23836–23841.
5 L. Jiang, W. Sun, Y. Gao and J. Zhao, *Phys. Chem. Chem. Phys.*, 2014, **16**, 6623–6629.
6 S. Jiang, Y. Zhang, Y. Gan, Z. Chen and H. Peng, *J. Phys. D: Appl. Phys.*, 2013, **46**, 335302.
7 R. Huang, G.-F. Shao, X.-M. Zeng and Y.-H. Wen, *Sci. Rep.*, 2014, **4**, 2045.
8 Z. Shan, G. Adesso, A. Cabot, M. Sherburne, S. S. Asif, O. Warren, D. Chrzan, A. Minor and A. Alivisatos, *Nature Mater.*, 2008, **7**, 947–952.
9 L. Yang, J. Bian, H. Zhang, X. Niu and G. Wang, *AIP Adv.*, 2015, **5**, 077162.
10 Z. Yang, X. Zheng and J. Zheng, *J. Electrochem. Soc.*, 2016, **163**, B466–B470.
11 L. Dubau, J. Durst, F. Maillard, L. Guétaz, M. Chatenet, J. André and E. Rossinot, *Electrochim. Acta*, 2011, **56**, 10658–10667.
12 S. J. Son, X. Bai and S. B. Lee, *Drug Discov. Today*, 2007, **12**, 650–656.
13 S. J. Son, X. Bai and S. B. Lee, *Drug Discov. Today*, 2007, **12**, 657–663.

14 H. Liu, F. Ye and J. Yang, *Indust. & Eng. Chem. Res.*, 2014, **53**, 5925–5931.

15 S. E. Fioressi, D. E. Bacelo, G. Bozzolo, H. O. Mosca and M. F. del Grosso, *Comp. Mater. Sci.*, 2015, **98**, 142–148.

16 A. N. Enyashin and A. L. Ivanovskii, *J. Molecular Structure: THEOCHEM*, 2007, **822**, 28–32.

17 C. Ji and H. S. Park, *Nanotechnology*, 2007, **18**, 115707.

18 F. Delogu, *J. Phys. Chem. C*, 2008, **112**, 11135–11143.

19 J. Yin, M. Retsch, J.-H. Lee, E. L. Thomas and M. C. Boyce, *Langmuir*, 2011, **27**, 10492–10500.

20 H. Akbarzadeh, E. Mehrjouei, A. N. Shamkhali, M. Abbaspour, S. Salemi and S. Ramezanzadeh, *J. Phys. Chem. Lett.*, 2017, **8**, 5064.

21 H. Akbarzadeh, E. Mehrjouei, A. N. Shamkhali, M. Abbaspour, S. Salemi and S. Ramezanzadeh, *Inorg. Chem. Front.*, 2017, **4**, 1679–1690.

22 Z. Yan, R. Bao, R. N. Wright and D. B. Chrisey, *Applied Physics Letters*, 2010, **97**, 124106.

23 Z. Yan, R. Bao and D. B. Chrisey, *Nanotechnology*, 2010, **21**, 145609.

24 Z. Yan, R. Bao, C. M. Busta and D. B. Chrisey, *Nanotechnology*, 2011, **22**, 265610.

25 R. Sen, A. Govindaraj, K. Suenaga, S. Suzuki, H. Kataura, S. Iijima and Y. Achiba, *Chemical physics letters*, 2001, **340**, 242–248.

26 S. Li, M. Chen and X. Liu, *Optics express*, 2014, **22**, 18707–18714.

27 S. J. Kim, C. S. Ah and D.-J. Jang, *Adv. Mater.*, 2007, **19**, 1064–1068.

28 V. T. Karpukhin, M. M. Malikov, T. I. Borodina, G. E. Valyano, O. A. Gololobova and D. A. Strikanov, *High Temperature*, 2015, **53**, 93–98.

29 G. González-Rubio, P. Díaz-Núñez, A. Rivera, A. Prada, G. Tardajos, J. González-Izquierdo, L. Bañares, P. Llombart, L. G. Macdowell, M. A. Palafox *et al.*, *Science*, 2017, **358**, 640–644.

30 S. Plimpton, *J. Comp. Phys.*, 1995, **117**, 1 – 19.

31 M. S. Daw and M. I. Baskes, *Phys. Rev. B*, 1984, **29**, 6443.

32 H. Sheng, M. Kramer, A. Cadien, T. Fujita and M. Chen, *Phys. Rev. B*, 2011, **83**, 134118.

33 J. Tersoff, *Phys. Rev. B*, 1989, **39**, 5566.

34 J. Yu, S. B. Sinnott and S. R. Phillpot, *Phys. Rev. B*, 2007, **75**, 085311.

35 A. Stukowski, *Model. Simul. Mater. Sc.*, 2010, **18**, 015012.

36 A. Stukowski, *Model. Simul. Mater. Sc.*, 2012, **20**, 045021.

37 S. Ramos de Debiaggi, E. A. Crespo, F. Braschi, E. Bringa, M. Alí and M. Ruda, *Int. J. Hydrogen Energy*, 2014, **39**, 8590–8595.

38 X. Zhou, R. Johnson and H. Wadley, *Phys. Rev. B*, 2004, **69**, 144113.

39 R. Johnson, *Phys. Rev. B*, 1989, **39**, 12554.

40 S. Foiles, M. Baskes and M. S. Daw, *Phys. Rev. B*, 1986, **33**, 7983.

41 G. Nie, X. Lu, J. Lei, L. Yang, X. Bian, Y. Tong and C. Wang, *Electrochim Acta*, 2013, **99**, 145 – 151.

42 J. W. Hong, S. W. Kang, B.-S. Choi, D. Kim, S. B. Lee and S. W. Han, *ACS Nano*, 2012, **6**, 2410–2419.

43 Y. Si, M. Chen and L. Wu, *Chem. Soc. Rev.*, 2016, **45**, 690–714.

44 Y.-N. Tan, J. Yang, J. Y. Lee and D. I. Wang, *J. Phys. Chem. C*, 2007, **111**, 14084–14090.

45 B. Y. Xia, H. B. Wu, X. Wang and X. W. Lou, *J. Amer. Chem. Soc.*, 2012, **134**, 13934–13937.